Chelating ligands as electrolyte solvent for rechargeable zinc-ion batteries

Vivek Verma,[†] R Moesha Chan,[†] Li Jia Yang,[†] Sonal Kumar,[†] Suchinda Sattayaporn,[‡] Rodney Chua,[†] Yi Cai,[†] Pinit Kidkhunthod,[‡] William Manalastas Jr,[†] and Madhavi Srinivasan*[,†,¶]

†*School of Materials Science and Engineering, Nanyang Technological University, 11 Faculty Ave, Singapore 639977*

‡*Synchrotron Light Research Institute (Public Organization), Muang, Nakhon Ratchasima, 30000, Thailand*

¶*Energy Research Institute @ NTU (ERI@N), Nanyang Technological University, Research Techno Plaza, 50 Nanyang Drive, Singapore 637553, Singapore*

E-mail: madhavi@ntu.edu.sg

Abstract

Rechargeable zinc-ion batteries (RZIBs) are mostly powered by aqueous electrolytes. However, uncontrolled water interactions often confer a small voltage window and poor battery capacity retention. Here, we explore replacing water with ethylene glycol as the primary solvent in zinc electrolyte formulations. The assembled batteries reveal suppressed electrolyte-induced parasitic reactions, leading to: 1) expanded voltage stability windows up to 2.2 V, 2) prolonged zinc stripping/plating stability up to 2.4 times longer compared to the water-based counterparts, and 3) doubled cathode capacity retentions as observed in full-cell Zn-$FeVO_4$ RZIBs. Using a combination of synchrotron EXAFS and FTIR, we investigate the molecular level salt-solvent interactions and explain how

the chelation ability of EG ligands reduces parasitic reactions to enable the enhanced electrochemical performances. The structural insights should provide guidelines on the selection of salt, concentration and chelating solvents for robust multivalent-ion battery systems.

Introduction

Multivalent-ion batteries can be a promising technology for grid-scale energy storage as multivalent metals like Mg, Zn, Ca, Al are abundant, environmentally benign and safer to handle than Li.[1–7] Among the various multivalent metal choices, zinc metal as an anode offers many advantages: 1) it has a higher volumetric capacity than Li, Ca and Mg.[4] 2) Zn metal has been demonstrated to reversibly strip/plate in aqueous electrolytes unlike the other multivalent metals (Mg, Ca, Al).[1,8] However, the zinc electrolytes developed in the literature suffer from many problems, thus making a robust rechargeable zinc ion battery (RZIB) still remains a challenge.[8,9]

Most RZIB studies utilize aqueous electrolytes. However, high water contents create three major problems. Firstly, as we demonstrate, the voltage windows of conventional aqueous zinc electrolytes are limited to $\sim$ 1.7 V. A small voltage window can lead to continuous electrolyte decomposition while cycling high voltage cathode materials.[8,10] There have been many attempted strategies to resolve this by increasing the zinc salt concentrations in water.[11] However, the limited zinc salt solubility still results in abundant "free water" molecules in the system, thus making voltage window expansion of the electrolytes difficult.[9,11] Secondly, at the zinc metal anode, the aqueous electrolytes decompose via a competitive hydrogen evolution process during the zinc plating process. This gas evolution can lead to a pressure build up inside the cell and can ultimately lead to cell failure.[12,13] Thirdly, the abundant free water molecules in the aqueous electrolytes can dissolve the cathode materials during the RZIB operation especially at slower current rates, thus leading to a capacity fade.[8,14] Therefore, as the electrolyte solvent is such a crucial factor in determining

the salt solubility and the electrochemical voltage window,[15,16] exploring electrolyte solvents beyond water could be one strategy to make better RZIB electrolytes.

As a solvent, polar protic molecules which double as hydrogen bond donors can dissolve large amounts of multivalent compounds due to the strong Lewis/Brønsted acid-base interactions of these molecules with multivalent cations.[17–19] Additionally, some candidates in this electrolyte class may exhibit a wide electrochemical voltage window along with suppressed hydrogen evolution.[12,17] Based on these considerations, we explore ethylene glycol (EG), one of the simplest hydrogen bond donors, as a solvent for zinc electrolytes. Like water, EG has: 1) O-H groups; 2) a high polarity and dielectric constant; 3) a high affinity to donate electron pairs (donor number[20]) (Table 1). Moreover, there is previous evidence that EG can dissolve large amounts of multivalent-ion salts.[19,21] To the best of our knowledge, EG has only been explored as an electrolyte additive for RZIBs[22–24] and not as a primary solvent for zinc or other multivalent-ion battery electrolytes.

In this study, we investigate ethylene glycol as an electrolyte solvent for two zinc salts, namely zinc triflate ($Zn(OTf)_2$) and zinc chloride ($ZnCl_2$). The choice of the salt anions were made considering their coordination strengths: the OTf^- ($CF_3SO_3^-$) anion has a very weak coordination strength, while the Cl^- anion is highly electronegative and strongly coordinating.[26,27] Therefore, the two extreme anion classes can provide a general illustration of EG behavior as a solvent with zinc salts. We measure the physical properties of the formulated electrolytes including maximum salt solubility, thermal phase transitions, ionic conductivity,

Table 1: Solvent properties of ethylene glycol and water.

Solvent	Formula	M.P.	B.P.	D_N	ϵ	μ
Water	H_2O	0	100	18	80.2	1.85
Ethylene Glycol	$(CH_2\text{-}OH)_2$	-12.6	197.3	20	41.4	2.36

M.P. and B.P are melting and boiling points in °C; D_N: donor number; ϵ: dielectric constant; μ: polarity in Debye. Values taken from ref[20,25]

viscosity and electrochemical stability voltage window. We then evaluate the suitability of pairing these electrolytes with zinc metal anodes by galvanostatic stripping/plating tests in symmetric Zn|Zn cells. We finally demonstrate a full-cell RZIB consisting of an EG-based electrolyte, Zn metal anode and a $FeVO_4$ cathode and show the benefits of EG-based electrolytes compared to conventional water-based electrolytes.

Furthermore, the physico-electrochemical properties of the electrolytes have been shown to depend on the salt-solvent interactions and more specifically on the metal coordination sphere.[15,28,29] Hence, we characterize the structure of the zinc coordination sphere in-depth using FTIR (Fourier Transform-Infrared Spectroscopy) and EXAFS (Extended X-ray Absorption Fine Structure) techniques. Through the structural characterization, we explore how the competition between the salt anion and the EG solvent dictates the Zn^{2+} coordination sphere and the findings should aid the design of other multivalent-ion electrolytes using chelating solvents.

Experimental Details

Electrolyte Preparation: All the electrolytes were made in an ambient atmosphere condition. Before using ethylene glycol (EG) for any purpose, the solvent was first kept in molecular sieves (3 Å) for one day to dry out any absorbed moisture. To make the electrolytes, the salts zinc triflate ($Zn(OTf)_2$) (98% Sigma Aldrich) or zinc chloride (anhydrous, 98% Sigma Aldrich) were weighed in the appropriate amounts. The zinc salts were added to EG and heated to 60 °C with continuous stirring for at least 5 h. These electrolytes were then stored in glass vials with molecular sieves.

Physical Properties Measurements: The Differential scanning calorimetry measurements were carried out using Q10 DSC instrument (TA instruments) at a heating/cooling rate of 5 °C/min. The samples were cooled from room temperature to -80 °C and then again heated till 40 °C. The viscosity of the electrolytes were measured using a Brookfield DV3T

Rheometer with spindle-52 at 25 °C with 0.5 mL of electrolyte samples. Specific ionic conductivities were measured using a conductivity cell with a cell constant of 1.01 cm^{-1} (Orion 3 Star, Thermoelectron Corporation, USA) at room temperature. The water content of the electrolytes were measured using a CA-200 Coulometric Karl Fischer Titrator (Mitsubishi Chemical). The cationic transference number was calculated in a symmetric Zn|Zn cell using the Bruce-Vincent method[30] in Biologic SP-200 electrochemical workstation. The EIS spectra were measured before and after a constant voltage polarization of 5 mV (ΔV) for 18 hours to find the initial and steady-state passivating layer resistance, R_o and R_s respectively. The resistance values were found by fitting the EIS spectra in the EC-lab (Biologic) software. The initial current (I_o) and the steady state current (I_s) are also noted in the constant voltage polarization process. Using the following formula, the Zn transference number can be calculated: $T = (I_S(\Delta V - I_o R_o))/(I_o(\Delta V - I_s R_S))$. The voltage window was measured in a three-electrode setup using Linear Sweep Voltammetry (LSV) with symmetric Ti|Ti electrodes as the working/counter electrodes and Ag/AgCl as the reference electrode, at a scan rate of 3 mV/s using a Biologic SP-200 electrochemical workstation. LSV scans were made with a negative sweep followed by a positive sweep on the same Ti electrodes. The cut-off current density for determination of voltage window was kept at 1 $\mu A/cm^2$ to account for electrolyte decomposition in a real working battery.[31]

Electrolyte Structural characterization: The Fourier Transform Infrared Resonance (FTIR) spectra were measured in ATR (attenuated total reflectance) mode using a Nicolette iS50 ATR (Thermo Scientific) for the range 500 to 4000 cm^{-1} with a resolution of 2 cm^{-1} and averaged over 32 scans. EXAFS measurements were carried out for the Zn K-edge at the Beamline 5.2, Synchrotron Light Research Institute, Thailand in fluorescence mode. The electron energy was 1.2 GeV, beam current 80-150 mA, and the maximum photon flux was about 1.1-1.7 $\times$ 10^{11} photons s^{-1}. Germanium (220) double single crystals were utilized as a monochromator. For each sample, the measurement was carried out for 5 times with a maximum k up to 12 $Å^{-1}$. The background subtraction was done using the Athena program,

and the EXAFS data were fitted using the Artemis program. The $S_o{}^2$ value was estimated to be 0.61 using a standard 2m $Zn(OTf)_2$/water solution.

Electrochemical Characterization: The Zn stripping/plating and the full cell Zn-$FeVO_4$ RZIB electrochemical performances were evaluated using 2016-type coin cells. To make the coin cells, a glass fibre (Whatmann) separator soaked in the appropriate electrolyte was sandwiched between the working and the counter electrodes. All the coin cells were assembled in an ambient atmosphere environment. In the case of Zn stripping/plating test, the working and the counter electrodes were zinc foil disks (16 mm diameter, Goodfellow). For the Zn-$FeVO_4$ RZIB system, the counter electrodes and working electrodes were zinc foil disks and the $FeVO_4$ electrodes, respectively. To make the $FeVO_4$ electrodes, $FeVO_4$ active material was used which was developed by our group previously.[32] A slurry of the $FeVO_4$ active material, PVDF binder, and super P carbon was made in a weight ratio of 6:2:2 in N-methyl-2-pyrrolidone solvent. The slurry was coated on a Ti foil and the coated Ti foil was vacuum dried overnight before using it in the coin cell. The mass loadings of the active material were $\sim$ 1-1.3 mg per electrode. A BTS Neware battery testing system was used for galvanostatic charge-discharge studies.

Ex-Situ characterization: XRD patterns were collected using a Bruker D8 Advance diffractometer in Bragg-Brentano geometry. Here, XRD patterns of the zinc foils after aging in the appropriate electrolytes were acquired. XRD patterns of the zinc foils after Zn stripping/plating tests were also acquired, after opening the coin cells, rinsing the Zn foils with DI water and drying in air. The SEM micrographs of the zinc foils were obtained using a Field Emission SEM (JEOL, JSM-7600F).

Results and discussion

Physical Property Characterization

Salt solubility

The salts $Zn(OTf)_2$ and $ZnCl_2$ show high solubilities in the EG solvent. Stable compositions of the $Zn(OTf)_2$:EG system can be made up to a salt:solvent molar ratio of 1:5 (fig 1a). Notably, the dissolved salt solubility in EG is higher by 2.4 times than in water and 4.7 times than in acetonitrile solvents (which corresponds to saturation concentrations of 4 m in water and 1 m in acetonitrile).[16,33] On the other hand, stable compositions of the $ZnCl_2$: EG system can be made up to the ratio 1:3 (fig 1a). Notably, the $ZnCl_2$ solubility achieved is higher than that of $Zn(OTf)_2$ in EG as also observed in water solvent.[14] However, the maximum $ZnCl_2$ solubility in EG is slightly lower than the $ZnCl_2$ in water (1:3 vs 1:1.8).[34] The high solubility in water has been ascribed to the transition of the $ZnCl_2$-H_2O system to a molten salt or hydrated melt state at near saturation salt concentrations.[35,36]

These saturated EG-based electrolytes remain stable in the liquid state without any solidification/crystallization even after 10 months in sealed conditions (fig S1). The water content after 10 months was measured to be $\sim$ 1.2-1.4 % by weight (Karl Fischer titration). The high liquid stability of these electrolytes is also reflected in the DSC measurements as no crystallization or freezing processes were observed down to temperatures as low as -80 °C (fig 1b). This suppressed crystallization behavior has also been observed in EG-based electrolytes with alkali metal salts,[37] and consistent with the popular antifreeze properties of EG. On the other hand, the conventional water-based electrolytes are prone to crystallization at subzero temperatures (fig S2).

Ionic conductivity and viscosity

The ionic conductivities and the viscosities were measured for the $Zn(OTf)_2$/EG and the $ZnCl_2$/EG systems (fig 1c & 1d). The ionic conductivities of the $Zn(OTf)_2$ and $ZnCl_2$

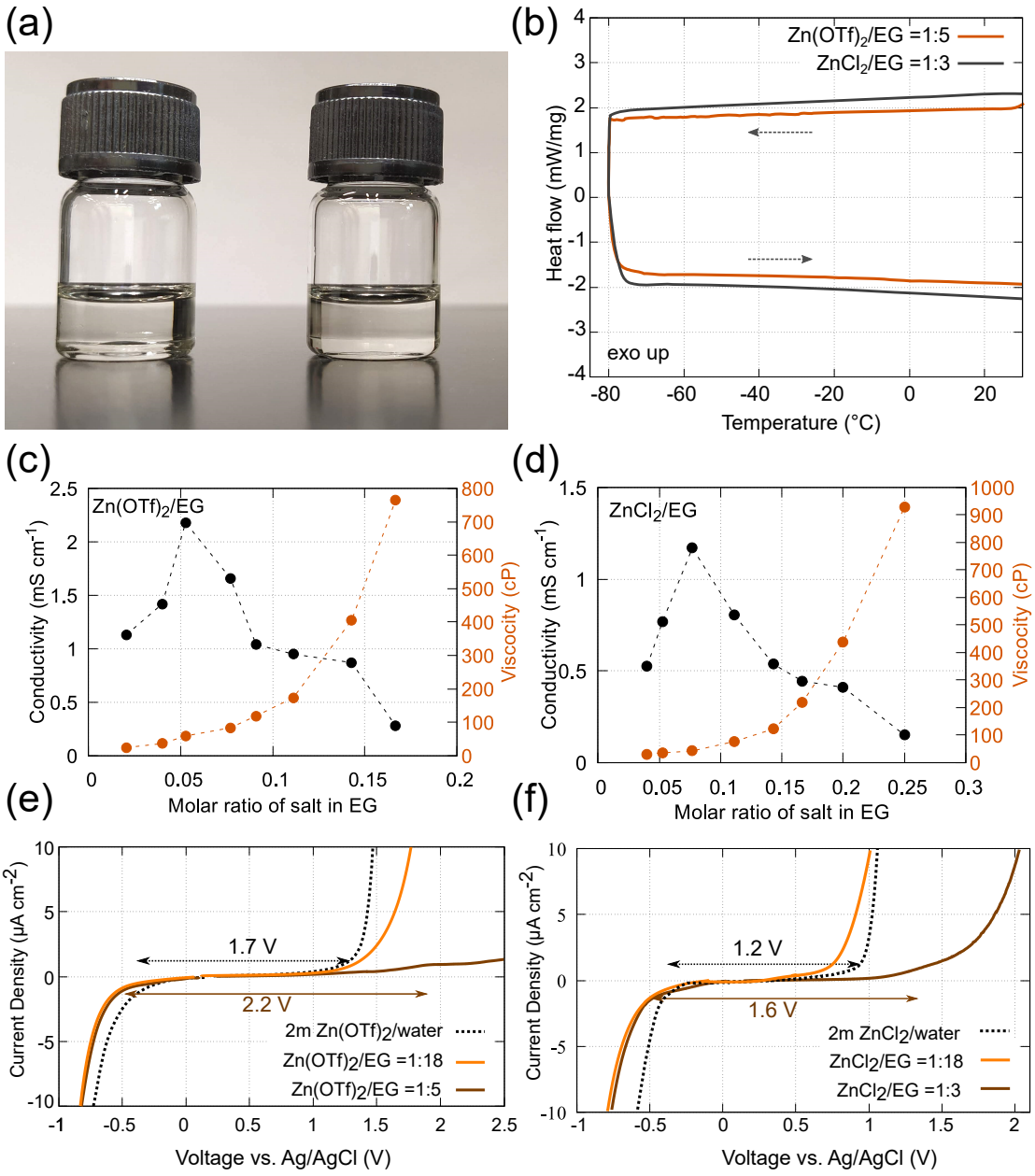

Figure 1: Physical properties of the ethylene glycol-based electrolytes. (a) Electrolytes prepared with maximum salt to solvent ratio for $ZnCl_2$ (left) and $Zn(OTf)_2$ (right). (b) DSC cooling and heating data for the electrolytes at scan rate of 5 °C/min. Ionic conductivity and viscosity trends with varying molar ratio of salt to solvent in (c) $Zn(OTf)_2$/EG and (d) $ZnCl_2$/EG systems. Electrochemical voltage window at a scan rate of 3 mV/s for (e) $Zn(OTf)_2$ in EG and $Zn(OTf)_2$ in water (f) $ZnCl_2$ in EG and $ZnCl_2$ in water.

electrolyte series lies in the range of 0.1 to 2.5 mS/cm. Although this range of conductivity values is an order lower than aqueous and non-aqueous zinc electrolytes, it is still higher than the polymer-based zinc electrolytes (Table S1). Moreover, on increasing the salt : solvent

ratio, the ionic conductivity values increase initially, reach a maximum, and then drop down again (fig 1c & 1d). This trend is consistent with the trends in the ionic conductivity and viscosity observed in other high salt concentration electrolytes and the reasons will be explored later in this work.[38,39] Furthermore, the contributions from the Zn^{2+} ions in the total ionic conductivity was estimated from the transference number (fig S3). The transference number for saturated $Zn(OTf)_2$ and $ZnCl_2$ electrolytes were found to be 0.52 and 0.44 respectively, and are around the same values for other zinc-based hydrogen bond donor electrolytes developed previously ($\sim$ 0.5-0.6).[12,40] Notably, the value for $ZnCl_2$ is lower than $Zn(OTf)_2$ electrolyte which can be ascribed to a suppressed zinc cation mobility because of the strong Zn-Cl interactions as shown later in our work.[15]

Electrochemical stability

The electrochemical stability of the electrolytes was studied for the dilute and concentrated $Zn(OTf)_2$/EG and $ZnCl_2$/EG systems (fig 1e & 1f). For comparison, the voltage windows were also measured for $Zn(OTf)_2$ and $ZnCl_2$ salts in water solvents. In dilute EG electrolytes, the voltage windows obtained are either similar to or smaller than the water-based counterparts. On the other hand, when zinc salt concentrations are increased to near saturation levels in EG, the electrolyte decomposition during the oxidation step is suppressed, similar to other zinc electrolytes with hydrogen bond donors.[12] As a result, an expanded voltage stability window of $\sim$ 2.2 V for $Zn(OTf)_2$ in EG and $\sim$ 1.6 V for $ZnCl_2$ in EG can be realized. We also note that the cathodic electrolyte stability window in the reduction sweep improves only marginally in EG solvent as compared to water solvent. This can be ascribed to the fact that the negative current during the reduction sweep in the zinc electrolytes has a combined contribution from two simultaneous reduction processes: 1) the electrolyte solvent decomposition via hydrogen evolution reaction (HER) and, 2) the Zn^{2+} reduction to Zn metal.[41] Therefore, even if the HER process is suppressed, the zinc deposition process will still give rise to the negative current in the reduction sweep and the cathodic

voltage window improvement will appear to improve only marginally. Nevertheless, we will demonstrate later in our work that HER reaction is indeed suppressed (see electrochemical characterization section) . Notably, the voltage windows of the $ZnCl_2$ electrolytes are lower than their $Zn(OTf)_2$ counterparts regardless of using EG or water as the solvent. This lower electrolyte stability window can be ascribed to the fact that chloride ions are susceptible to oxidize to Cl_2 gas during the oxidation step.[1,42]

The reason for the trends in ionic conductivity, viscosity and electrochemical voltage stability window in EG solvents should lie in the salt-solvent interactions. Therefore, we study the salt and solvent interactions using FTIR and EXAFS techniques.

Structural Characterization

FTIR

In pure EG solvent without the addition of any salt, the IR absorption peaks appear at 3300, 1083, 1033, 882 and 860 cm^{-1} as shown by the vertical dotted lines in fig 2. The peak at 3300 cm^{-1} represents the O-H stretching vibrations; 1083 cm^{-1} and 1033 cm^{-1} represent the C-O stretching; and, 882 cm^{-1} and 860 cm^{-1} represent CH_2 rocking and C-C stretching, respectively.[43] As we add the $Zn(OTf)_2$ salt and increase its concentration, we observe shifts in the peak positions as follows.

Firstly, on increasing the salt concentration, the intensity of the O-H vibration peak reduces (fig 2a), indicating that the fraction of the free or uncoordinated EG solvent molecules is reducing.[44,45] Moreover, the peak becomes broader and shifts to a lower wavenumber, as also observed during the bonding of EG molecules with multivalent ions.[21,46] Secondly, we see a red shift in the C-O vibration peaks (fig 2b), a phenomenon consistent with the peak shifts observed for the analogous Ni and Co complexes with EG.[47,48] The red shift of the C-O vibration peaks indicates a weakening of the C-O bonds.[21,46] This shift is expected when the electron lone pairs of the O atoms from the EG molecule are used to form bonds with the Zn^{2+} metal ions (fig 2d). Moreover, at any of the salt:solvent ratio, apart from the vibrations

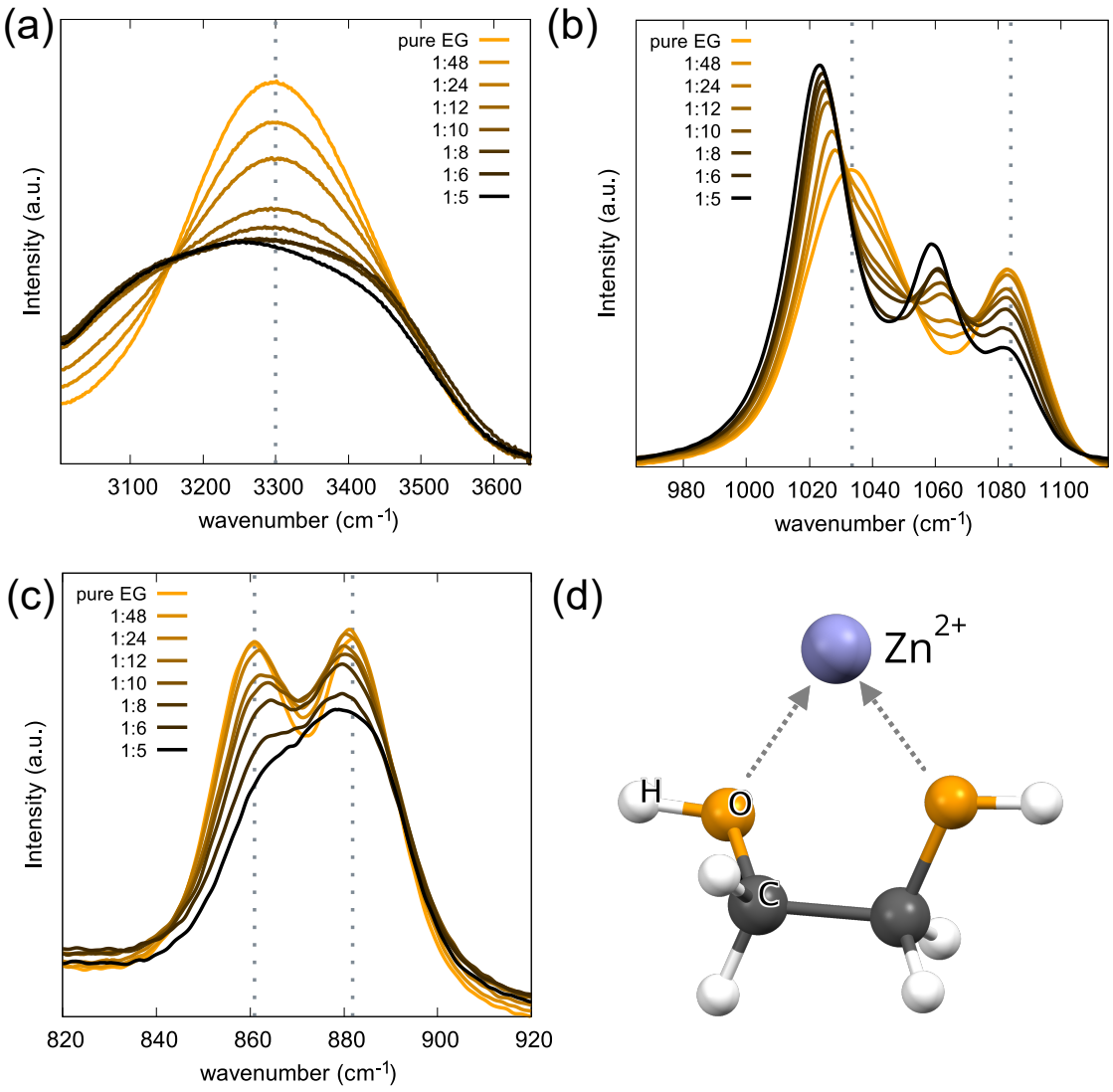

Figure 2: (a), (b), (c) The evolution of the FTIR spectrum upon increasing the $Zn(OTf)_2$:EG molar ratio. The dotted vertical lines indicate the peak positions in the pure EG solvent. (d) Schematic showing the bidentate ligand coordination between EG and Zn^{2+}.

of free/unbonded EG (dotted lines in fig 2b), the two newly emerging C-O vibration peaks are single peaks without any peak splitting or shoulder peaks (fig 2b). This implies that both the O atoms from the EG molecule are in identical environments and therefore, the EG molecule binds to the Zn^{2+} center in a bidentate way (fig 2d).[21,49] Finally, since the newly formed Zn-O bond affects the C atoms in the EG molecule, the C-C and the C-H bonds will also be perturbed. Therefore, the C-C stretching peaks and the CH_2 rocking peaks also shift as observed during metal-ligand formation with EG (fig 2c).[21]

All the trends in the FTIR peak shifts observed here in the $Zn(OTf)_2$/EG system have also been observed for the $ZnCl_2$/EG system (fig S4). Therefore, these trends indicate that not only can EG form a bidentate metal-ligand bond in the presence of a weakly-coordinating anion like OTf^- but also in the presence of a strong anion like Cl^-. Studying the coordination environment around the Zn^{2+} in $Zn(OTf)_2$/EG and $ZnCl_2$/EG systems will further elucidate the Zn^{2+}-EG bonding mechanism and therefore we investigate the coordination environment around the Zn^{2+} ions using the EXAFS technique.

EXAFS

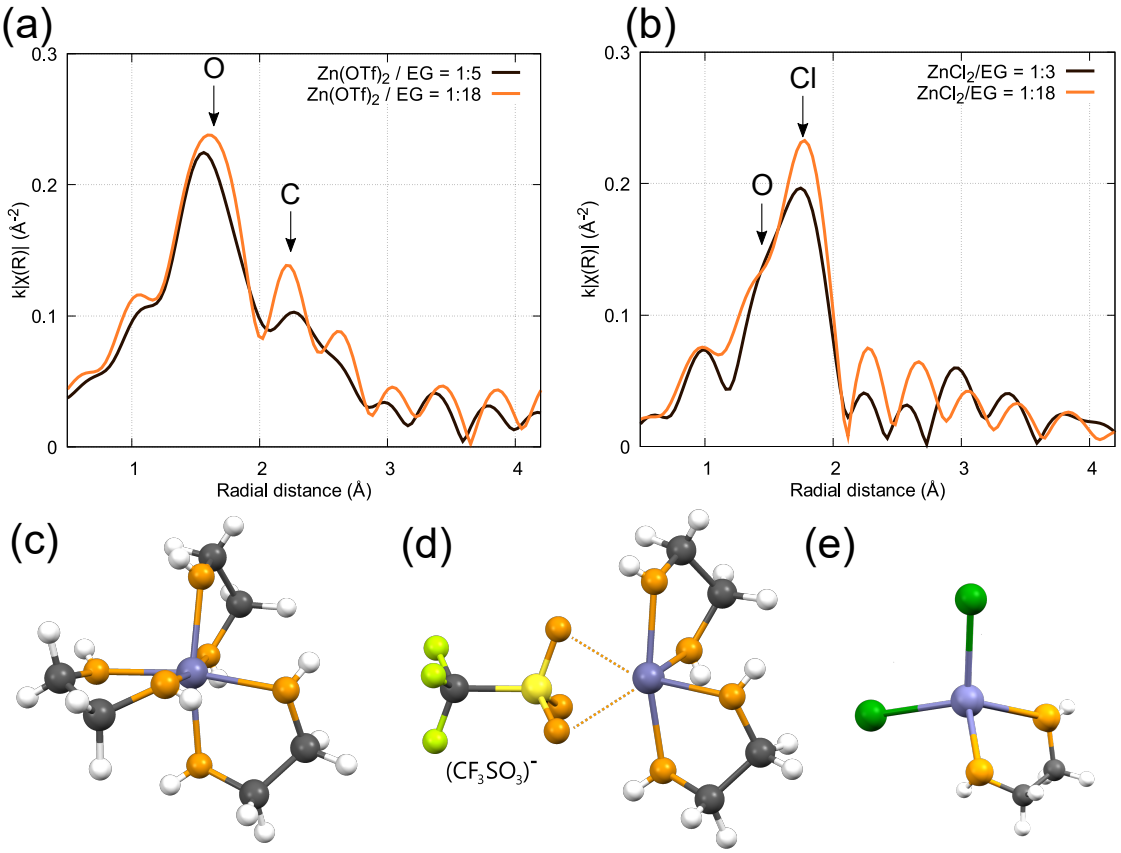

Figure 3: Fourier transform EXAFS signals for the (a) $Zn(OTf)_2$/EG and (b) $ZnCl_2$/EG systems. Schematics representing the Zn^{2+} coordination structure in the $Zn(OTf)_2$/EG systems at the salt:solvent ratio of (c) 1:18 and (d) 1:5. The colors of the sphere represent purple: Zn, orange: O, black: C, white: H. (e) Schematic of the average Zn^{2+} coordination structure in the $ZnCl_2$/EG salt:solvent ratio of 1:18; the green spheres indicate chlorine atoms

The EXAFS technique can elucidate the local atomic arrangement around the Zn^{2+} ion center. Here, the X-ray photons bombard the sample with energies sufficient to knock off a core electron from the atoms of the probed element (Zn^{2+}). The knocked-off electron (or photoelectron) wave can be scattered off from the different surrounding atoms located at different distances. These scattered waves can return to the Zn^{2+} center and modulate the probability of X-ray absorption at the Zn^{2+} ion center. Thus, a rough atomic arrangement around the Zn^{2+} center can be deduced.[50] The Fourier transform EXAFS signals for the zinc K-edge for the $Zn(OTf)_2$ and $ZnCl_2$ systems at low and high salt concentrations are shown in fig 3. Briefly, every coordination shell composed of equidistant atoms from Zn^{2+} will give rise to high-intensity peaks in the EXAFS spectrum and the peak position (in Å) is related to the shell distance from the Zn^{2+} center (or bond lengths). The peak intensity is proportional to the scattering strength which depends on 1) the number of atoms present in the shell (or coordination number for the first shell), and 2) the atomic number of the scattering element. We also note that the coordination environment elucidated by the EXAFS analysis is an average of all the Zn^{2+} coordination environments in the whole sample. All four spectra of the EG based electrolytes have one feature in common, that is no large peaks are observed at radial distances beyond ∼3.5 Å (fig 3a and 3b). Hence, beyond a radial distance of roughly 3.5 Å from Zn^{2+} center, the atoms are randomly arranged and lack a long-range order. However, short-range ordering is observed close to the Zn^{2+} in all the systems (fitting details in Table 2 and fig S5) as discussed below.

$Zn(OTf)_2$/EG system:

For the $Zn(OTf)_2$/EG system at low concentration (1:18) (fig 3a), a big peak at 1.6 Å from the first shell is observed and can be attributed to nearly 6 oxygen atoms with a Zn-O bond distance of ∼2.07 Å.[52] The estimated Zn-O bond distance of 2.07 Å appears slightly different from the 1.6 Å shown in the fig 3a since the radial distances after the Fourier transform of the EXAFS data will be slightly shifted than the actual radial distribution functions due to the phase shifts.[50] These O atoms present in the first coordination sphere belong to the EG

Table 2: EXAFS fitting details for the electrolytes

Sample	**Element**	**N** $^{\alpha}$	$\boldsymbol{R}$**(Å)** $^{\beta}$	ΔE_o **(eV)** $^{\gamma}$	σ^2 $^{\epsilon}$	**R-factor** $^{\zeta}$
$Zn(OTf)_2$/EG (1:18)	O	5.6 $^{\delta}$	2.072	8.268	0.004	0.007
	C	5.2 $^{\delta}$	2.865	8.268	0.007	
$Zn(OTf)_2$/EG (1:5)	O	5.5 $^{\delta}$	2.076	8.362	0.005	0.003
	C	3.8	2.894	8.362	0.005	
$ZnCl_2$/EG (1:18)	Cl	2.4	2.223	1.253	0.003	0.001
	O	1.8	2.083	1.253	0.002	
$ZnCl_2$/EG (1:3)	Cl	2.1	2.215	-1.323	0.002	0.018
	O	1.4	2.073	-1.323	0.003	

$^{\alpha}$ number of atoms; $^{\beta}$ distance from Zn^{2+} ion center; $^{\gamma}$ energy shift when k=0; $^{\epsilon}$ mean-square disorder in R; $^{\zeta}$ fractional misfit; $^{\delta}$ the number of atoms appears less than 6 in the fitting since second shell C peak has large contribution to the first shell O atoms and is consistent with previous EXAFS fitting on similar systems.[18,51]

molecules and not to the OTf^- anion for three reasons. Firstly, other studies have shown that EG is a stronger ligand and can displace all OTf^- anions attached to divalent cations like Ni^{2+} or Cu^{2+}.[53,54] Secondly, a shoulder peak at 2.2 Å can also be observed (fig 3a). This type of EXAFS spectrum was also observed in a complex of Ni^{2+} with three EG ligand molecules roughly arranged in the way shown in fig 3c.[18] The shoulder peak could be fitted to roughly to 6 C atoms at an average distance of ∼2.8 Å.[18] Finally, using X-ray diffraction studies, Antti et al. and Teichert et al have demonstrated that Zn^{2+} coordination to three EG ligands is indeed feasible.[27,55] Therefore, we conclude that 3 EG molecules chelate the Zn^{2+} ion center as shown in fig 3c.

In contrast, when we increase the $Zn(OTf)_2$ salt concentration to 1:5, the EXAFS spectrum could be fitted with roughly 6 O atoms in the first shell and only 4 C atoms in the second shell. A reduction in the number of C atoms from 6 to 4 indicates that on average, only 2 EG molecules now coordinate to the Zn^{2+} center. This trend is expected as we deprive the system of free EG molecules and is consistent with the FTIR results.

This reduction in the extent of solvent molecule coordination has also been previously

observed where Zn^{2+} was coordinated by other hydrogen bond donors.[12,56] These previous studies found that on increasing the salt:solvent ratio, the salt anion entered the Zn^{2+} coordination sphere. Consistent with these previous studies, we can deduce that the observed value of ∼6 O atoms in the first coordination shell might have contributions from the O atoms of the OTf^- ($CF_3SO_3^-$) anion. Since 4 out of the 6 O atoms are from the EG solvent as discussed previously, the remaining 2 O atoms are most likely contributed by the OTf^- anion, and on an average we expect roughly one OTf^- anion to coordinate to the Zn^{2+} as shown in fig 3d.

$ZnCl_2$/EG system:

The $ZnCl_2$/EG system behaves differently to the $Zn(OTf)_2$/EG system, and this can be ascribed to the fact that the halide ions are highly electronegative compared to the weakly coordinating OTf^- anion and are tightly bound to the Zn^{2+}.[27,39] This is evident in the EXAFS signal where we can see both Cl and O atoms contribute to the first shell peak of the Zn^{2+} ion center (fig 3b). For the 1:18 ratio, the EXAFS spectrum could be fitted with roughly 2 Cl atoms and 2 O atoms at a distance of 2.3 Å and 2.07 Å respectively. Since, the EG solvent is expected to attach as a bidentate ligand from our FTIR results, the Zn^{2+} coordination structure should appear like in fig 3e. Therefore, the EG solvation mechanism involves undissociated Zn-Cl bonds and only 1 EG molecule could bind to the Zn^{2+} center. This is unlike the case for $Zn(OTf)_2$/EG system where, for the same salt:solvent ratio of 1:18, all salt anions were stripped off the Zn^{2+} ion center and 3 EG molecules could bind to the Zn^{2+} center.

On increasing the salt concentration to 1:3, the EXAFS fitting shows that the overall coordination number (both Cl and O) in the first shell reduces from ∼4 to ∼3.5. The reduction in the coordination numbers to values less than 4 is consistent with the other systems involving high concentrations of $ZnCl_2$.[57] This trend indicates that the fraction of Zn^{2+} centers which form zinc-chloro complexes or polymeric species are increasing.[39,57,58] Although the structural details with high $ZnCl_2$ concentrations in similar systems are not

fully understood yet,[39,58,59] the formation of zinc-chloro complexes indicates that Cl^- ions coordination dominates over EG on increasing the Cl^-:EG molar fraction in the system. Notably, the chelation of Zn^{2+} center of the zinc salts by EG solvent differs from their aprotic counterpart glyme solvents studied previously and the differences are briefly discussed in the supporting information (Note S1).

Structure-physicochemical properties correlation

The structural findings between Zn salts and EG can explain the trends in the physicochemical properties discussed in the previous section. For both the $Zn(OTf)_2$ and $ZnCl_2$ cases, as we increase the salt concentration in EG, we can make the following inferences regarding the viscosity and the ionic conductivity. Firstly, as the available EG molecules in the system reduce and most of the solvent molecules are used up in coordinating with Zn^{2+}, the fraction of the uncoordinated or "free" EG solvent molecules reduce. Consistent with the trend in most other concentrated electrolytes developed,[15,39,60] a reduction in the available free solvent molecules will increase the viscosity (fig 1c,1d). Secondly, in terms of conductivity, we observe that the conductivity initially increases, reaches a maximum and then decreases again. This behaviour is also consistent with other concentrated electrolytes developed.[38,60] On increasing the salt concentrations initially, we increase the mobile charge carriers which increases the conductivity. However, further increasing the charge carriers beyond a limit might increase the ion-pairing/aggregation rather than mobile free ions as also observed in other concentrated electrolytes.[60] The increased ion aggregation along with the rise in the viscosity will reduce the ion mobility, and hence the conductivity decreases (fig 1c,1d).[15,39]

Furthermore, at saturation levels of the zinc salt concentrations, most of the EG molecules form coordination bonds with the Zn^{2+} ion center by donating their electron lone pairs from O to Zn^{2+}. A similar bonding phenomenon has also been observed by Yoshida et al. between the O atoms of glyme solvent molecules and Li^+.[61] The reduction of the electron density of O

atoms will lower the highest occupied molecular orbital (HOMO) level of the EG molecules. Simultaneously, the shortage of free/uncoordinated EG solvent molecules at near saturation salt concentrations also reduces their activity.[29] These two factors will result in enhancing the electrochemical voltage window of the EG electrolytes at higher salt concentrations (fig 1e,1f).

To explore the application of these saturated EG electrolytes in RZIBs, we investigate the electrochemical performance of these systems in the following section.

Electrochemical characterization

As a first step to check the feasibility of using the EG-based electrolytes in RZIB, we examined the chemical stability of the zinc metal in these electrolytes and compare it with the conventional aqueous electrolytes. We dip zinc foils in either the EG or water-based electrolytes for three weeks and investigate the phases on the zinc metal surface (fig S7). In the case of water-based electrolytes, we see that a white passivation layer forms on the zinc foil surface. Moreover, we also detect the formation of a new phase in the XRD pattern (fig S7c,d) . These results are similar to the previous studies on zinc foil aging in aqueous $ZnSO_4$ or $ZnClO_4$ electrolytes, wherein basic zinc salts (BZS) precipitated on the zinc foil surface.[62,63] Indeed, the new phases in our aged foils could also be indexed to the BSZ $Zn_x(OTf)_y(OH)_{2x-y}.nH_2O$ (in $Zn(OTf)_2$) and $Zn_5(OH)_8Cl_2.H_2O$ (in $ZnCl_2$) (fig S7c,d).[64–66] We discuss more about these phases later in this work. These phases are expected to form because: 1) the aqueous electrolytes are mildly acidic and produce H_2 gas spontaneously when in contact with the zinc metal.[4,13] 2) As a result of the consumption of the protons, the pH of the electrolytes will rise and the electrolyte salts will precipitate out.[65,67] The corresponding reactions can be written in the following equations.[63]

$$Zn \longrightarrow Zn^{2+} + 2\,e^{-} \tag{1}$$

$$2\,H_2O + 2\,e^- \longrightarrow H_2 + 2\,OH^- \tag{2}$$

$$(\text{in aq } ZnCl_2)\ 5\,Zn^{2+} + 8\,OH^- + 2\,Cl^- + H_2O \longrightarrow Zn_5(OH)_8Cl_2 \cdot H_2O; \text{or} \tag{3a}$$

$$(\text{in aq } Zn(OTf)_2)\ \ xZn^{2+} + (2x-y)OH^- + yOTf^- + nH_2O \longrightarrow Zn_x(OTf)_y(OH)_{2x-y} \cdot nH_2O \tag{3b}$$

On the other hand, no such phases in XRD were observed when zinc foils are aged in the EG-based electrolytes. This trend can be expected as unlike aqueous electrolytes, the EG-based electrolytes have almost negligible water content; and previous studies have shown that reducing or eliminating the electrolyte water content suppresses the BZS precipitation as water molecules are a crucial component to form these phases.[22,66,68]

To investigate if the EG based electrolytes can support a reversible zinc stripping/plating with a zinc metal anode, we perform the galvanostatic stripping/plating in symmetric Zn|Zn cells using these electrolytes. At a current density of 0.5 mA/cm^2 and 1 h deposition intervals (0.5 mAh/cm^2 per half cycle), $Zn(OTf)_2$/EG system could cycle for more than 600 h, or nearly 2.4 times longer than $Zn(OTf)_2$/water system (fig 4a). A similar trend was also observed in the case of $ZnCl_2$ where the cell could run for 250 h, or 2.7 times longer than the water counterpart (fig S8a). Notably, the overpotential in the EG-based electrolytes observed is higher when compared to their water counterparts. This can be ascribed to lower ionic conductivities in EG-based electrolytes and this trend is consistent with zinc electrolytes developed with other hydrogen bond donors.[12] Nevertheless, the overpotential profiles in the EG electrolytes remain smooth without large fluctuations. On the other hand, the water-based electrolytes either showed very high overpotentials (fig 4a), or the overpotentials dropped to nearly zero indicative of short-circuiting (fig S8a).[69] Additionally, when the coin cells were examined visually after this test, the coin cells with EG-based electrolytes were intact (fig S8b). On the other hand, the coin cells with water-based electrolytes either showed swelling or opened. This opening/swelling of coin cells has also been observed in cycling water-based electrolytes previously and can be ascribed to electrolyte decomposition

and hydrogen gas evolution.[12,13] To further investigate the failure mechanism during the zinc stripping/plating tests, we carry out the post-mortem XRD and SEM analysis of the cycled zinc foils.

In the case of $Zn(OTf)_2$/EG electrolyte, the optical image of the zinc foil and the separator shows that the separator remains intact (fig 4b). The SEM image of the zinc foil shows that the zinc foil deposition occurs in granular morphology (fig 4b), and the XRD pattern appears very similar to the fresh zinc foil (fig 4d). On the other hand, the optical image of the cell cycled in $Zn(OTf)_2$/water electrolyte gives a clear evidence that the zinc dendrites grow and can even pierce the separator (fig 4c). The SEM image of the zinc foil shows that a plate like morphology grows on the zinc foil. Moreover, this cycled zinc foil shows a new phase in the XRD pattern (fig 4d). The new phase can be ascribed to the BZS of $Zn(OTf)_2$ discussed previously. This phase has also been observed in RZIBs with $Zn(OTf)_2$/water electrolytes, however, it is not well characterized.[64,70] The BZS is a common family of zinc salts where $Zn(OH)_6$ units form sheets which sandwiches water and the salt anion molecules like Cl^-, NO_3^-, CH_3COO^- etc.[68] Similar to the BZS with acetate anions,[68] the obtained OTf based BZS can be indexed to a hexagonal phase with a= 7.023(3) Å and c =13.456(1) Å. This layered BZS phase as expected will grow as sheets as also observed in the SEM image. On the similar lines, the $ZnCl_2$/water system also shows $Zn_5(OH)_8Cl_2.H_2O$ BZS phase (ICSD 01-074-3156)[71] grows as sheets on the zinc foil which is suppressed in the EG solvent (fig S9). Therefore, EG based electrolytes can suppress the parasitic reactions such as electrolyte decomposition, dendrites and corrosion reactions during zinc stripping/plating which are commonly observed with water-based electrolytes.

Finally, to demonstrate the benefits of EG as an electrolyte solvent in a full cell RZIB, we compared the electrochemical performance of EG based electrolyte with a conventional water-based electrolyte using a Zn-$FeVO_4$ system. In the case of aqueous electrolytes, although we see a high discharge capacity of $\sim$ 250 mAh/g during the initial cycles, only 33.8 % of the initial capacity is retained after 100 cycles (fig 4e). This severe capacity fade has

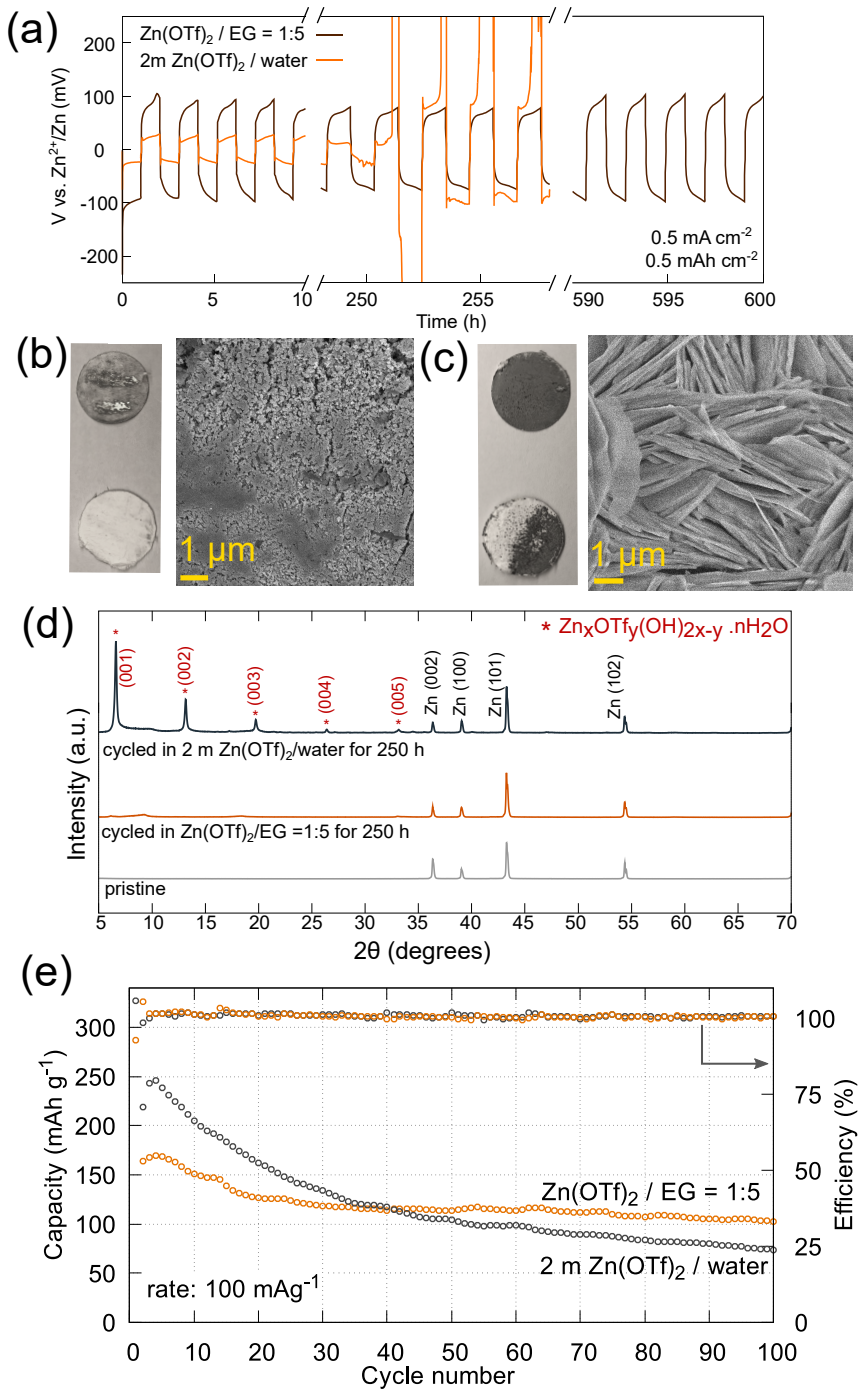

Figure 4: (a) Stripping/plating behavior of the electrolytes in symmetric Zn|Zn cell with $Zn(OTf)_2$ in EG and water. Optical image of the zinc foil (top) and the separator(bottom); and SEM micrograph of the zinc foils of with $Zn(OTf)_2$ salt in (b) EG and (c) water. (d) XRD pattern of the zinc foils post-cycling. (e) Comparative cycling performance for a full cell Zn-$FeVO_4$ battery with EG and water as solvent.

been ascribed to the cathode material dissolution caused by free water solvent molecules in aqueous electrolyte.[11,14,32,72] This cathode material dissolution is also reflected when the cathode material powder is stirred in the aqueous electrolyte for a week and the electrolyte solution turns colored as also observed with other vanadium based cathode materials in water-based electrolytes (fig S10).[14,73,74] In the case of EG-based electrolytes, we observe that the initial capacity is $\sim$ 170 mAh/g, which is lower compared to aqueous electrolytes. This is also reflected in the galvanostatic charge discharge curves of the two systems (fig S11). This can be ascribed to the slower kinetics due to a relatively low ionic conductivities of EG-based electrolytes as has also been observed with other hydrogen bond donor based zinc electrolytes.[12,13] However, a much improved capacity retention of 63% is observed; nearly two folds higher than when using water-based electrolytes. A similar improvement in the capacity retention has also been observed in electrolytes with near-saturation level of salts in water, and the reason has been previously ascribed to a reduced cathode material dissolution when the free/uncoordinated solvent molecules reduce.[72,75] Therefore, the saturated EG-based electrolytes mitigate the unwanted cathode-electrolyte interactions to improve the capacity retentions.

Conclusions

In this study, a polar protic solvent consisting of bidentate ligand molecules, ethylene glycol, was demonstrated as an effective electrolyte solvent for zinc salts. Not only can EG-based electrolytes be made in an ambient environment, but they also demonstrate a high shelf life of 10 months and can resist crystallization down to temperatures as low as -80 °C. Moreover, EG has high zinc salt solubilities and can stabilize salt:solvent molar ratios higher than 1:5. At the maximum salt concentrations, a drastic reduction in the free/uncoordinated EG solvent molecules suppresses electrolyte decomposition reactions which expands the anodic stability window. This enables operational voltage windows beyond those of conventional

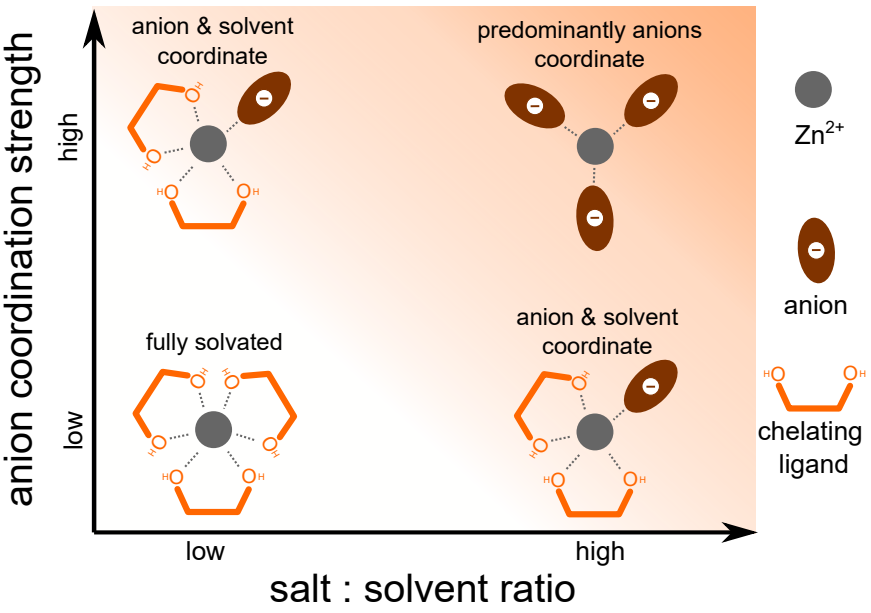

Figure 5: Schematic for the evolution of zinc coordination sphere as a function of salt: solvent ratio and the anion coordination strength

water-based electrolytes, up to 2.2.V.

From the RZIB perspective, the EG-based electrolytes mitigate the problems encountered in water-based electrolytes by reducing: 1) the electrolyte decomposition and gas evolution during the stripping/plating at the zinc metal anode, and 2) the capacity fade due to cathode material dissolution. Thus, capacity retention is improved by nearly two folds. EG is therefore found to be a promising electrolyte solvent, which should encourage further exploration of similar ligands for use in zinc electrolytes.

Finally, we demonstrate that the physico-electrochemical properties of these EG-based electrolytes are dependent on the way anions and the EG solvent molecules compete to bind with Zn^{2+} to form the Zn^{2+} coordination sphere. We elucidate that for a given chelating solvent like EG, the Zn^{2+} coordination sphere can be tuned when varying two crucial factors: 1) the zinc salt: solvent ratio and, 2) the anion coordination strength (fig 5). We demonstrate that with a chelating solvent like EG, full solvation of Zn^{2+} is feasible only when the anion is weakly coordinating ($CF_3SO_3^-$) and present in dilute concentrations. On the other extreme, when the anion is strongly coordinating (Cl^-) and present at very high concen-

trations, the Zn^{2+} is predominantly forming aggregates with the salt anions itself. For the other intermediate cases (fig 5), both the EG and the anion will coordinate with the Zn^{2+} ion center. Thus, these findings provide a guideline for estimating the coordination sphere of the multivalent cations when selecting the chelating solvent, salt and the salt concentration for multivalent-ion electrolytes (Zn, Mg, Ca, Al) where high salt cation-anion dissociation is desirable.

Acknowledgement

This work was funded by the National Research Foundation of Singapore Investigatorship Award Number NRFI2017-08. V. V thanks Disha Gupta for help with EXAFS analysis, Arun Nagasubramanian for help with conductivity measurements, and Rohit Satish & Sai S. H. Dintakurti for a fruitful discussion on structural analysis. The authors thank Synchrotron Light Research Institute (BL 5.2), Nakhon Ratchasima, Thailand for EXAFS measurements, and the Facility for Analysis, characterization, Testing and Simulation, NTU, Singapore, for use of their electron microscopy/X-ray facilities.

Supporting Information Available

The following files are available free of charge.

- Supporting information containing electrolyte stability photos, DSC data, FTIR for $ZnCl_2$/EG, fitted EXAFS data, Zn aging optical images and XRD data, Zn|Zn stripping/plating data and the associated post-mortem XRD and SEM analysis, charge-discharge curves for Zn-$FeVO_4$ system.

Conflict of interest

The authors declare no conflict of interest.

References

(1) Liang, Y.; Dong, H.; Aurbach, D.; Yao, Y. Current status and future directions of multivalent metal-ion batteries. *Nature Energy* **2020**, 1–11.

(2) Canepa, P.; Sai Gautam, G.; Hannah, D. C.; Malik, R.; Liu, M.; Gallagher, K. G.; Persson, K. A.; Ceder, G. Odyssey of multivalent cathode materials: open questions and future challenges. *Chemical reviews* **2017**, *117*, 4287–4341.

(3) Verma, V.; Kumar, S.; Manalastas Jr, W.; Satish, R.; Srinivasan, M. Progress in Rechargeable Aqueous Zinc-and Aluminum-Ion Battery Electrodes: Challenges and Outlook. *Advanced Sustainable Systems* **2019**, *3*, 1800111.

(4) Manalastas Jr, W.; Kumar, S.; Verma, V.; Zhang, L.; Yuan, D.; Srinivasan, M. Water in rechargeable multivalent-ion batteries: an electrochemical Pandora's box. *ChemSusChem* **2018**, *12*, 379–396.

(5) Yuan, D.; Zhao, J.; Manalastas, W.; Kumar, S.; Srinivasan, M. Emerging rechargeable aqueous aluminum ion battery: Status, challenges, and outlooks. **2020**, *2*, 248 – 263.

(6) Kumar, S.; Satish, R.; Verma, V.; Ren, H.; Kidkhunthod, P.; Manalastas Jr, W.; Srinivasan, M. Investigating $FeVO_4$ as a cathode material for aqueous aluminum-ion battery. *Journal of Power Sources* **2019**, *426*, 151–161.

(7) Chua, R.; Cai, Y.; Kou, Z. K.; Satish, R.; Ren, H.; Chan, J. J.; Zhang, L.; Morris, S. A.; Bai, J.; Srinivasan, M. 1.3 V superwide potential window sponsored by Na-Mn-O plates as cathodes towards aqueous rechargeable sodium-ion batteries. *Chemical Engineering Journal* **2019**, *370*, 742–748.

(8) Blanc, L. E.; Kundu, D.; Nazar, L. F. Scientific Challenges for the Implementation of Zn-Ion Batteries. *Joule* **2020**, *4*, 771 – 799.

(9) Huang, S.; Zhu, J.; Tian, J.; Niu, Z. Recent Progress in the Electrolytes of Aqueous Zinc-Ion Batteries. *Chemistry–A European Journal* **2019**, *25*, 14480–14494.

(10) Li, Q.; Ma, K.; Yang, G.; Wang, C. High-voltage non-aqueous $Zn/K_{1.6}Mn_{1.2}Fe(CN)_6$ batteries with zero capacity loss in extremely long working duration. *Energy Storage Materials* **2020**, *29*, 246 – 253.

(11) Zhang, H.; Liu, X.; Li, H.; Hasa, I.; Passerini, S. Challenges and Strategies for High-Energy Aqueous Electrolyte Rechargeable Batteries. *Angewandte Chemie* **2020**, 10.1002/anie.202004433.

(12) Qiu, H.; Du, X.; Zhao, J.; Wang, Y.; Ju, J.; Chen, Z.; Hu, Z.; Yan, D.; Zhou, X.; Cui, G. Zinc anode-compatible in-situ solid electrolyte interphase via cation solvation modulation. *Nature communications* **2019**, *10*, 1–12.

(13) Zhao, J.; Zhang, J.; Yang, W.; Chen, B.; Zhao, Z.; Qiu, H.; Dong, S.; Zhou, X.; Cui, G.; Chen, L. "Water-in-deep eutectic solvent" electrolytes enable zinc metal anodes for rechargeable aqueous batteries. *Nano Energy* **2019**, *57*, 625–634.

(14) Ni, Q.; Jiang, H.; Sandstrom, S.; Bai, Y.; Ren, H.; Wu, X.; Guo, Q.; Yu, D.; Wu, C.; Ji, X. A $Na_3V_2(PO_4)_2O_{1.6}F_{1.4}$ Cathode of Zn-Ion Battery Enabled by a Water-in-Bisalt Electrolyte. *Advanced Functional Materials* **2020**, 2003511, 10.1002/adfm.202003511.

(15) Rajput, N. N.; Seguin, T. J.; Wood, B. M.; Qu, X.; Persson, K. A. *Modeling Electrochemical Energy Storage at the Atomic Scale*; Springer, 2018; pp 79–124.

(16) Han, S.-D.; Rajput, N. N.; Qu, X.; Pan, B.; He, M.; Ferrandon, M. S.; Liao, C.; Persson, K. A.; Burrell, A. K. Origin of electrochemical, structural, and transport properties in nonaqueous zinc electrolytes. *ACS applied materials & interfaces* **2016**, *8*, 3021–3031.

(17) Smith, E. L.; Abbott, A. P.; Ryder, K. S. Deep eutectic solvents (DESs) and their applications. *Chemical reviews* **2014**, *114*, 11060–11082.

(18) Hartley, J. M.; Ip, C. M.; Forrest, G. C.; Singh, K.; Gurman, S. J.; Ryder, K. S.; Abbott, A. P.; Frisch, G. EXAFS study into the speciation of metal salts dissolved in ionic liquids and deep eutectic solvents. *Inorg. Chem.* **2014**, *53*, 6280–6288.

(19) Abbott, A. P.; Barron, J. C.; Ryder, K. S.; Wilson, D. Eutectic-Based Ionic Liquids with Metal-Containing Anions and Cations. *Chemistry - a European Journal* **2007**, *13*, 6495–6501.

(20) Marcus, Y. The effectivity of solvents as electron pair donors. *Journal of solution chemistry* **1984**, *13*, 599–624.

(21) Knetsch, D.; Groeneveld, W. Alcohol as ligands. III. Complexes of Ethylene glycol with some divalent metal halides. *Inorganica Chimica Acta* **1973**, *7*, 81–87.

(22) Wang, N.; Yang, Y.; Qiu, X.; Dong, X.; Wang, Y.; Xia, Y. Stabilized Rechargeable Aqueous Zinc Batteries Using Ethylene Glycol as Water Blocker. *ChemSusChem* **2020**, *13*, 5556–5564.

(23) Chang, N.; Li, T.; Li, R.; Wang, S.; Yin, Y.; Zhang, H.; Li, X. An aqueous hybrid electrolyte for low-temperature zinc-based energy storage devices. *Energy & Environmental Science* **2020**, *13*, 3527–3535.

(24) Qin, R.; Wang, Y.; Zhang, M.; Wang, Y.; Ding, S.; Song, A.; Yi, H.; Yang, L.; Song, Y.; Cui, Y., et al. Tuning Zn2+ coordination environment to suppress dendrite formation for high-performance Zn-ion batteries. *Nano Energy* **2020**, 105478.

(25) Haynes, W. M. *CRC handbook of chemistry and physics*; CRC press, 2014; pp 1145–1427.

(26) Taube, H.; Scott, A. Complexing tendency of trifluoromethylsulfonate ion as measured using chromium (III). *Inorganic Chemistry* **1971**, *10*, 62–66.

(27) Teichert, J.; Ruck, M. Influence of Common Anions on the Coordination of Metal Cations in Polyalcohols. *Eur. J. Inorg. Chem.* **2019**, *2019*, 2267–2276.

(28) Mandai, T.; Johansson, P. Haloaluminate-free cationic aluminum complexes: structural characterization and physicochemical properties. *The Journal of Physical Chemistry C* **2016**, *120*, 21285–21292.

(29) Suo, L.; Borodin, O.; Tao, G.; Olguin, M.; Ho, J.; Fan, X.; Chao, L.; Wang, C.; Kang, X. "Water-in-salt"electrolyte enables high-voltage aqueous lithium-ion chemistries. *Science* **2015**, *350*, 938–943.

(30) Evans, J.; Vincent, C. A.; Bruce, P. G. Electrochemical measurement of transference numbers in polymer electrolytes. *Polymer* **1987**, *28*, 2324–2328.

(31) Kuhnel, R.-S.; Reber, D.; Battaglia, C. Perspective—Electrochemical Stability of Water-in-Salt Electrolytes. *Journal of The Electrochemical Society* **2020**, *167*, 070544.

(32) Kumar, S.; Verma, V.; Chua, R.; Hao, R.; Kidkhunthod, P.; Rojviriya, C.; Sattayaporn, S.; de Groot, F. M.; Manalastas, W. J.; Srinivasan, M. Multiscalar Investigation of $FeVO_4$ Conversion Cathode for a Low Concentration $Zn(CF_3SO_3)_2$ Rechargeable Zn-ion Aqueous Battery. *Batteries & Supercaps* **2020**, *3*, 619–630.

(33) Zhang, N.; Cheng, F.; Liu, Y.; Zhao, Q.; Lei, K.; Chen, C.; Liu, X.; Chen, J. Cation-deficient spinel $ZnMn_2O_4$ cathode in $Zn(CF_3SO_3)_2$ electrolyte for rechargeable aqueous Zn-ion battery. *Journal of the American Chemical Society* **2016**, *138*, 12894–12901.

(34) Zhang, C.; Holoubek, J.; Wu, X.; Daniyar, A.; Zhu, L.; Chen, C.; Leonard, D. P.; Rodríguez-Pérez, I. A.; Jiang, J.-X.; Fang, C., et al. A ZnCl 2 water-in-salt electrolyte for a reversible Zn metal anode. *Chemical communications* **2018**, *54*, 14097–14099.

(35) Wilcox, R. J.; Losey, B. P.; Folmer, J. C.; Martin, J. D.; Zeller, M.; Sommer, R. Crystalline and liquid structure of zinc chloride trihydrate: a unique ionic liquid. *Inorganic chemistry* **2015**, *54*, 1109–1119.

(36) Angell, C.; Sare, E. Glass-forming composition regions and glass transition temperatures for aqueous electrolyte solutions. *The Journal of Chemical Physics* **1970**, *52*, 1058–1068.

(37) Cruz, H.; Jordão, N.; Amorim, P.; Dionísio, M.; Branco, L. C. Deep eutectic solvents as suitable electrolytes for electrochromic devices. *ACS Sustainable Chemistry & Engineering* **2018**, *6*, 2240–2249.

(38) Yamada, Y.; Wang, J.; Ko, S.; Watanabe, E.; Yamada, A. Advances and issues in developing salt-concentrated battery electrolytes. *Nature Energy* **2019**, *4*, 269–280.

(39) Kar, M.; Winther-Jensen, B.; Forsyth, M.; MacFarlane, D. R. Exploring zinc coordination in novel zinc battery electrolytes. *Physical Chemistry Chemical Physics* **2014**, *16*, 10816–10822.

(40) Narayanan, N. V.; Ashokraj, B.; Sampath, S. Physicochemical, electrochemical, and spectroscopic characterization of zinc-based room-temperature molten electrolytes and their application in rechargeable batteries. *Journal of The Electrochemical Society* **2009**, *156*, A863.

(41) Han, C.; Li, W.; Liu, H. K.; Dou, S.; Wang, J. Principals and strategies for constructing a highly reversible zinc metal anode in aqueous batteries. *Nano Energy* **2020**, *74*, 104880.

(42) Zhang, Y.; Chen, Z.; Qiu, H.; Yang, W.; Zhao, Z.; Zhao, J.; Cui, G. Pursuit of reversible Zn electrochemistry: a time-honored challenge towards low-cost and green energy storage. *NPG Asia Materials* **2020**, *12*, 1–24.

(43) Krishnan, K.; Krishnan, R. Raman and infrared spectra of ethylene glycol. Proceedings of the indian academy of sciences-section A. 1966; p 111.

(44) Chen, S.; Lan, R.; Humphreys, J.; Tao, S. Salt-concentrated acetate electrolytes for a high voltage aqueous Zn/MnO_2 battery. *Energy Storage Materials* **2020**, *28*, 205 – 215.

(45) Chua, R.; Cai, Y.; Lim, P. Q.; Kumar, S.; Satish, R.; Manalastas, W. J.; Ren, H.; Verma, V.; Meng, S.; Morris, S., et al. Hydrogen-Bonding Interactions in Hybrid Aqueous/Non-Aqueous Electrolyte Enables Low-Cost and Long-Lifespan Sodium-Ion Storage. *ACS Applied Materials & Interfaces* **2020**, *12*, 22862–22872.

(46) Knetsch, D.; Groeneveld, W. Alcohols as ligands: Part IV. Complexes of ethylene glycol with some metal (II) sulfates and nitrates. *Recueil des Travaux Chimiques des Pays-Bas* **1973**, *92*, 855–864.

(47) Labádi, I.; Kenessey, G.; Liptay, G. Preparation, thermoanalytical and IR study of mixed ligand complexes formed in water-1,2-ethanediol-nickel (II)-sulfate systems. *Journal of thermal analysis and calorimetry* **2005**, *82*, 55–61.

(48) Labádi, I.; Horváth, L.; Kenessey, G.; Liptay, G. Preparation, thermoanalytical and IR study of mixed-ligand complexes formed in water-1,2-ethanediol-cobalt(II)sulfate systems. *Journal of thermal analysis and calorimetry* **2006**, *83*, 247–251.

(49) Miyake, A. Infrared spectra of glycols coordinated to metal ions. *Bulletin of the Chemical Society of Japan* **1959**, *32*, 1381–1383.

(50) Calvin, S. *XAFS for Everyone*; CRC press, 2013; pp 3–27.

(51) Solvation structure of a copper(II) ion in protic ionic liquids comprising n-hexylethylenediamine. *Inorg. Chem.* **2014**, *53*, 9667–9678.

(52) D'Angelo, P.; Zitolo, A.; Ceccacci, F.; Caminiti, R.; Aquilanti, G. Structural characterization of zinc(II) chloride in aqueous solution and in the protic ionic liquid ethyl ammonium nitrate by x-ray absorption spectroscopy. *J. Chem. Phys.* **2011**, *135*, 1–8.

(53) Okan, S. E.; Salmon, P. S. The Jahn-Teller effect in solutions of flexible molecules: a neutron diffraction study on the structure of a Cu^{2+} solution in ethylene glycol. *Molecular Physics* **1995**, *85*, 981–998.

(54) Okan, S. E.; Salmon, P. S.; Champeney, D. C.; Petri, I. The solvation of cations in hydrogen-bonded molecular solvents: A neutron diffraction study on the structure of Ni^{2+} solutions in ethylene glycol and in glycerol. *Mol. Phys.* **1995**, *84*, 325–343.

(55) Antti, B.-M. The Molecular and Crystal Structure of Tris(1,2-ethanediol)-zinc(II) Sulfate: $[Zn(C_2H_6O_2)_3)SO_4]$. *Acta Chemica Scandinavica A 30* **1976**, *7*, 103–108.

(56) Fujita, T.; Yamaguchi, T.; Ohtaki, H. An X-Ray Diffraction Study on the Structures of Bis-and Tris (ethylenediamine) zinc (II) Complexes in Solution. *Bulletin of the Chemical Society of Japan* **1979**, *52*, 3539–3544.

(57) Zou, Y.; Xu, H.; Wu, G.; Jiang, Z.; Chen, S.; Huang, Y.; Huang, W.; Wei, X. Structural analysis of $[ChCl]_m[ZnCl_2]_n$ ionic liquid by x-ray absorption fine structure spectroscopy. *J. Phys. Chem. B* **2009**, *113*, 2066–2070.

(58) Kruh, R. F.; Standley, C. L. An X-Ray Diffraction Study of Aqueous Zinc Chloride Solutions. *Inorg. Chem.* **1962**, *1*, 941–943.

(59) Yamaguchi, T.; Hayashi, S. I.; Ohtaki, H. X-ray diffraction and Raman studies of zinc(II) chloride hydrate melts, $ZnCl_2 \cdot rH_2O$ (r = 1.8,2.5, 3.0,4.0, and 6.2). *J. Phys. Chem.* **1989**, *93*, 2620–2625.

(60) Yamada, Y.; Yamada, A. Superconcentrated electrolytes for lithium batteries. *Journal of The Electrochemical Society* **2015**, *162*, A2406–A2423.

(61) Yoshida, K.; Nakamura, M.; Kazue, Y.; Tachikawa, N.; Tsuzuki, S.; Seki, S.; Dokko, K.; Watanabe, M. Oxidative-stability enhancement and charge transport mechanism in glyme–lithium salt equimolar complexes. *Journal of the American Chemical Society* **2011**, *133*, 13121–13129.

(62) Yang, G.; Li, Q.; Ma, K.; Hong, C.; Wang, C. The degradation mechanism of vanadium oxide-based aqueous zinc-ion batteries. *Journal of Materials Chemistry A* **2020**, *8*, 8084–8095.

(63) Hao, J.; Li, X.; Zhang, S.; Yang, F.; Zeng, X.; Zhang, S.; Bo, G.; Wang, C.; Guo, Z. Designing Dendrite-Free Zinc Anodes for Advanced Aqueous Zinc Batteries. *Advanced Functional Materials* **2020**, 2001263.

(64) Oberholzer, P.; Tervoort, E.; Bouzid, A.; Pasquarello, A.; Kundu, D. Oxide versus nonoxide cathode materials for aqueous Zn batteries: an insight into the charge storage mechanism and consequences thereof. *ACS applied materials & interfaces* **2018**, *11*, 674–682.

(65) Jo, J. H.; Aniskevich, Y.; Kim, J.; Choi, J. U.; Kim, H. J.; Jung, Y. H.; Ahn, D.; Jeon, T.-Y.; Lee, K.-S.; Song, S. H., et al. New Insight on Open-Structured Sodium Vanadium Oxide as High-Capacity and Long Life Cathode for Zn–Ion Storage: Structure, Electrochemistry, and First-Principles Calculation. *Advanced Energy Materials* **2020**, 2001595.

(66) Yang, W.; Du, X.; Zhao, J.; Chen, Z.; Li, J.; Xie, J.; Zhang, Y.; Cui, Z.; Kong, Q.; Zhao, Z., et al. Hydrated Eutectic Electrolytes with Ligand-Oriented Solvation Shells for Long-Cycling Zinc-Organic Batteries. *Joule* **2020**, *4*, 1557–1574.

(67) Du, W.; Ang, E. H.; Yang, Y.; Zhang, Y.; Ye, M.; Li, C. Challenges in Material and Structure Design of Zinc Anode toward High-Performance Aqueous Zinc-Ion Batteries. *Energy & Environmental Science* **2020**, *13*, 3330–3360.

(68) Poul, L.; Jouini, N.; Fiévet, F. Layered hydroxide metal acetates (metal= zinc, cobalt, and nickel): elaboration via hydrolysis in polyol medium and comparative study. *Chemistry of Materials* **2000**, *12*, 3123–3132.

(69) Wang, L.; Zhang, Y.; Hu, H.; Shi, H.-Y.; Song, Y.; Guo, D.; Liu, X.-X.; Sun, X. A $Zn(ClO_4)_2$ Electrolyte Enabling Long-Life Zinc Metal Electrodes for Rechargeable Aqueous Zinc Batteries. *ACS applied materials & interfaces* **2019**, *11*, 42000–42005.

(70) Park, M. J.; Manthiram, A. Unveiling the Charge Storage Mechanism in Nonaqueous and Aqueous Zn/Na3V2 (PO4) 2F3 Batteries. *ACS Applied Energy Materials* **2020**, *3*, 5015–5023.

(71) Hawthorne, F. C.; Sokolova, E. Simonkolleite, $Zn_5(OH)_8Cl_2(H_2O)$, a decorated interrupted-sheet structure of the form [Mφ2]4. *The Canadian Mineralogist* **2002**, *40*, 939–946.

(72) Ao, H.; Chen, C.; Hou, Z.; Cai, W.; Liu, M.; Jin, Y.; Zhang, X.; Zhu, Y.; Qian, Y. Electrolyte solvation structure manipulation enables safe and stable aqueous sodium ion batteries. *J. Mater. Chem. A* **2020**, *8*, 14190–14197.

(73) Verma, V.; Kumar, S.; Manalastas Jr, W.; Zhao, J.; Chua, R.; Meng, S.; Kidkhunthod, P.; Srinivasan, M. Layered $VOPO_4$ as a Cathode Material for Rechargeable Zinc-Ion Battery: Effect of Polypyrrole Intercalation in the Host and Water Concentration in the Electrolyte. *ACS Applied Energy Materials* **2019**, *2*, 8667–8674.

(74) Mason, C. W.; Lange, F. Aqueous ion battery systems using sodium vanadium phosphate stabilized by titanium substitution. *ECS Electrochemistry Letters* **2015**, *4*, A79.

(75) Zheng, Q.; Miura, S.; Miyazaki, K.; Ko, S.; Watanabe, E.; Okoshi, M.; Chou, C.-P.; Nishimura, Y.; Nakai, H.; Kamiya, T., et al. Sodium-and potassium-hydrate melts containing asymmetric imide anions for high-voltage aqueous batteries. *Angewandte Chemie International Edition* **2019**, *58*, 14202–14207.

Graphical TOC entry